Electrochimica Acta 99 (2013) 211–218

Contents lists available at SciVerse ScienceDirect

Electrochimica Acta

journal homepage: www.elsevier.com/locate/electacta

Near-infrared and multicolored electrochromism of solution processable triphenylamine-anthraquinone imide hybrid systems

Fengkun Chen, Xiangyu Fu, Jie Zhang, Xinhua Wan*

Beijing National Laboratory for Molecular Sciences, Key Laboratory of Polymer Chemistry and Physics of Ministry of Education, College of Chemistry and Molecular Engineering, Peking University, Beijing 100871, China

ARTICLE INFO

Article history:
Received 8 February 2013
Received in revised form 8 March 2013
Accepted 10 March 2013
Available online xxx

Keywords:
Anthraquinone imide
Triphenylamine
Near-infrared
Multicolor electrochromism
Theoretical calculation

ABSTRACT

A series of novel donor-acceptor molecules (**TPA-AQI**, **TPA-AQI2** and **TPA-AQI3**) with various number of electron-accepting anthraquinone imide (AQI) arms connected to the electron-donating triphenylamine (TPA) core were synthesized and characterized by UV–vis absorption spectroscopy, cyclic voltammetry and spectroelectrochemical measurements. The geometries of these molecules in ground-state as well as the electronic absorption properties on the basis of the optimized geometries were investigated by theoretical calculations. For all the three molecules, there are two main absorptions in the range of 300–450 nm and 450–700 nm, respectively. The former corresponds to π—π^* transitions and the latter a nature of intramolecular charge transfer (ICT). Hypsochromic shift of the ICT absorption was observed from the single armed molecule **TPA-AQI** to the tribranched molecule **TPA-AQI3**, which may result from the increased steric hindrance between the donor and acceptor segments. Electrochemical studies revealed the ambipolar properties of these molecules and three redox couples, with two quasi-reversible redox couples appearing in the cathodic regime and one redox couple in the anodic regime, on CV curves. CV results also indicated the stabilization of the HOMO levels by increasing AQI arms. Spectroelectrochemical measurements demonstrated the near-infrared (NIR) and multicolor electrochromism of these molecules. When reduced to radical anions or oxidized to radical cations, intense NIR absorptions were observed accompanied with color changes of the solutions. As for **TPA-AQI**, there existed four different colors at different redox states: Indian-red at the neutral state, bluish green at the radical cationic state, olive green at the radical anionic state, and dark blue at the dianion state. The detailed transitions of the observed NIR absorptions were also discussed.

1. Introduction

Electrochromism is well-known as the reversible color change of a material upon electrochemical oxidation or reduction [1,2], and electrochromic (EC) materials can be employed in numerous practical applications such as optical memory devices [3–5], smart windows [6–8], and color displays [9,10]. In spite of the fact that the earliest reported EC materials are mainly inorganic oxides (i.e., WO_3) [11], organic EC materials, such as bipyridiliums (viologens) [12] and especially conducting polymers [13,14], demonstrate several promising advantages over the former ones, such as large-scale processability, fast response time, high coloration efficiency and multiple colorations with the same material [15–21], as well as fine-tuning of the colors through chemical structure modification [22–25]. Recently, the interested optical changes of EC materials have been extended into the near-infrared (NIR; e.g., 760–2500 nm) region for their important military and civilian applications in fields such as telecommunications, biomedicine and even thermal control for buildings or spacecrafts [26–29].

Up to now, several types of organic NIR electrochromic materials are developed, mainly including transition metal complexes [30–32], aromatic quinones [33,34], and some conjugated polymers [35–38]. On the other hand, however, the electrochromic properties of these materials are mostly realized by electrochemical oxidation. Only a limited number of materials have been reported to achieve color changes relied on electrochemical reduction [33,34,39–41], due to the low environmental stability of the reduced forms and lack of depth understanding of the structure-property relationship for novel molecular design. We previously explored the electrochromic properties of a series of electron-deficient anthraquinone imide (AQI) and its derivatives, which usually exhibited NIR absorptions in the range of 700–1100 nm upon one-electron reduction [42–44]. It was demonstrated recently that the NIR absorption of AQI radical anions could be feasibly elongated to the range of 1100–1800 nm with a strong electron deficient substitution [45].

* Corresponding author. Tel.: +86 10 62754187; fax: +86 10 62751708.
E-mail address: xhwan@pku.edu.cn (X. Wan).

0013-4686/$ – see front matter © 2013 Elsevier Ltd. All rights reserved.
http://dx.doi.org/10.1016/j.electacta.2013.03.067

Triphenylamine (TPA) derivatives and TPA-containing polymers are well-known electron-rich compounds with three dimensional structures which are widely used as hole-transporting and photovoltaic materials [46–49]. In addition, triphenylamines can also easily be oxidized to form TPA cationic radicals accompanying with a noticeable change of coloration [50–53]. Liou et al. have intensively explored EC materials based on TPA-containing polyimides which show interesting multichromism, good reversibility and mechanical stability [54–57]. They also reported that the incorporation of electron-donating substituents such as methoxyl group at the *para*-position of phenyl groups of TPA unit could not only stabilize the TPA cationic radicals but also decrease the oxidation potential [58,59]. In the meanwhile, additional interesting properties could be expected by combining the different electron-rich and electron-deficient groups in one single molecule.

In this work, herein, we reported the synthesis and characterization of three star-shaped donor (D)-acceptor (A) molecules with different electron-deficient AQI arms connected to the electron-rich TPA core. The ambipolar character of these molecules was revealed by electrochemical and spectroelectrochemical studies and single layer EC device was fabricated. Upon oxidation to radical cations or reduction to radical anions, intense NIR absorptions were observed. Multicolor could also be achieved in one single material at different redox states, e.g., for **TPA-AQI**, Indian-red at the neutral state, bluish green at the radical cationic state, olive green at the radical anionic state, and dark blue at the dianion state. Furthermore, detailed electronic transitions of the neutral and radical absorptions were investigated by theoretical calculations.

2. Experimental

2.1. Materials & methods

All reagents were obtained from J&K, Aldrich, Acros and TCI Chemical Co., and used as received unless otherwise specified. The bromo substituted triphenyl amine derivatives, namely *p*-bromo-*N*,*N*-dimethoxyphenylaniline (**1a**), 4-bromo-*N*,*N*-bis(4-methoxyphenyl)aniline (**1b**) and tris(4-bromophenyl)amine (**1c**), were prepared following the reported procedures [60–62]. Tetrakis(triphenylphosphine)palladium(0) ($(PPh_3)_4Pd^0$) was synthesized in our lab. 6-Bromo substituted anthraquinone imide **4** was prepared following the previously reported procedure with slight modification of the *N*-alkyl chain [63].

^{1}H NMR and ^{13}C NMR spectra were measured on a Mercury plus 300 (300 MHz) or Bruker ARX400 (400 MHz) spectrometer at the ambient temperature with $CDCl_3$ as the solvent. Chemical shifts in ^{1}H and ^{13}C NMR were recorded in ppm with tetramethylsilane (0 ppm) and $CDCl_3$ (77 ppm) as standards, respectively. High-resolution mass spectra were recorded on a Bruker APEX IV Fourier transform ion cyclotron resonance mass spectrometer. Elemental analyses were performed on an Elementar Vario EL instrument. UV/Vis absorption spectra were recorded on a Perkin–Elmer lambda 35 spectrophotometer. Diffuse reflectance measurements on powders were carried out on a Shimadzu UV-3100 UV/Vis/NIR spectrophotometer.

2.2. Synthesis

2.2.1. General procedure A for synthesis of triphenylamine substituted boronic ester (Scheme 1)

4-Bromo substituted triphenylamine was dissolved in dry THF under nitrogen atmosphere and it was cooled to −78 °C. *n*-BuLi was added with syringe and kept at −78 °C for one hour. 2-Isopropoxy-4,4,5,5-tetramethyl-[1,3,2]dioxaborolane was added dropwise. After addition, the solution was allowed to warm up to room temperature for overnight reaction. After quenching of the reaction with ammonium chloride solution, the water layer was extracted with chloroform and the combined organic layer was dried over $MgSO_4$. After the remove of the solvent under reduced pressure, the residue was purified by silica gel column chromatography (petroleum ether/dichloromethane 1:1) to afford the product as white solids.

2.2.2. 4-Methoxy-N-(4-methoxyphenyl)-N-[4-(4,4,5,5-tetramethyl-1,3,2-dioxaborolan-2-yl)phenyl]benzenamine (**2a**)

Following general procedure A, **1a** (1.67 g, 4.3 mmol), *n*-BuLi (3 mL, 6.6 mmol) and 2-isopropoxy-4,4,5,5-tetramethyl-[1,3,2]dioxaborolane (1.09 g, 5.9 mmol) were stirred in dry THF (20 mL) overnight. Silica gel column chromatography afforded **2a** as white solids (0.62 g, 33%). ^{1}H NMR (300 MHz, $CDCl_3$): δ = 7.60 (br, 2H), 7.06 (br, 4H), 6.84 (d, J = 8.4 Hz, 6H), 3.80 (s, 6H), 1.32 ppm (s, 12H).

2.2.3. N-(4-methoxyphenyl)-4-(4,4,5,5-tetramethyl-1,3,2-dioxaborolan-2-yl)-N-[4-(4,4,5,5-tetramethyl-1,3,2-dioxaborolan-2-yl)phenyl]benzenamine (**2b**)

Following general procedure A, **1b** (2.17 g, 5.0 mmol), *n*-BuLi (6 mL, 13.2 mmol) and 2-isopropoxy-4,4,5,5-tetramethyl-[1,3,2]dioxaborolane (2.28 g, 12.2 mmol) were stirred in dry THF (50 mL) overnight. Silica gel column chromatography afforded **2b** as white solids (1.60 g, 61%). ^{1}H NMR (300 MHz, $CDCl_3$); δ = 7.66 (d, J = 8.1 Hz, 4H), 7.08 (d, J = 8.7 Hz, 2H), 7.03 (d, J = 8.4 Hz, 4H), 6.86 (d, J = 8.7 Hz, 2H), 3.81 (s, 3H), 1.33 ppm (s, 24H).

2.2.4. Tris[4-(4,4,5,5-tetramethyl-1,3,2-dioxaborolan-2-yl)phenyl]amine (**2c**)

Following general procedure A, **1c** (1.92 g, 4.0 mmol), *n*-BuLi (6 mL, 13.2 mmol) and 2-isopropoxy-4,4,5,5-tetramethyl-[1,3,2]dioxaborolane (2.46 g, 13.2 mmol) were stirred in dry THF (50 mL) overnight. Silica gel column chromatography afforded **2c** as white solids (1.60 g, 64%). ^{1}H NMR (300 MHz, $CDCl_3$): δ = 7.69 (d, J = 8.4 Hz, 6H), 7.09 (d, J = 8.4 Hz, 6H), 1.34 ppm (s, 36H).

2.2.5. General procedure B for synthesis of triphenylamine-anthraquinone imide product

To a mixture of 6-bromo substituted anthraquinone imide **4**, Na_2CO_3 and $Pd(PPh_3)_4$, compound **2**, toluene, ethanol and water were added under nitrogen. The reaction mixture was heated to reflux and kept for 6 h. After cooled to room temperature, the water layer was extracted with dichloromethane and the combined organic layer was dried over $MgSO_4$. Volatile solvent was removed under reduced pressure. Then, the raw product was purified by silica gel column chromatography (petroleum ether/dichloromethane 1:2) as solids.

2.2.6. N-(1-hexylheptyl)-6-[4-[bis(4-methoxyphenyl)amino]phenyl]-anthraquinone-2,3-dicarboxylic imide (**TPA-AQI**)

Following general procedure B, compound **4** (0.59 g, 1.1 mmol), Na_2CO_3 (0.40 g, 3.8 mmol), $Pd(PPh_3)_4$ (60 mg) and compound **2a** (0.57 g, 1.4 mmol) were refluxed in a mixture of benzene (15 mL), ethanol (3 mL) and water (6 mL) under nitrogen. Silica gel column chromatography afforded the product **TPA-AQI** (0.47 g, 56%) as red solids. ^{1}H NMR (400 MHz, $CDCl_3$): δ = 8.77 (s, 2H), 8.53 (d, J = 2.0 Hz, 1H), 8.38 (d, J = 8.4 Hz, 1H), 8.04 (q, J_1 = 8.4, J_2 = 2.0 Hz, 1H), 7.59 (d, J = 8.8 Hz, 2H), 7.14 (d, J = 8.8 Hz, 4H), 7.02 (d, J = 8.4 Hz, 2H), 6.90 (d, J = 9.2 Hz, 4H), 4.32–4.23 (m, 1H), 3.83 (s, 6H), 2.14–2.05 (m, 2H), 1.78–1.70 (m, 2H), 1.32–1.23 (m, 16H), 0.86 ppm (t, J = 6.8 Hz, 6H); ^{13}C NMR (100 MHz, $CDCl_3$): δ = 182.0, 181.1, 167.0, 156.5, 150.0, 147.3, 140.0, 138.4, 138.1, 135.6, 135.4, 133.5, 131.8, 130.8, 128.6,

127.9, 127.3, 124.7, 122.4, 119.6, 55.5, 53.2, 32.3, 31.7, 28.9, 26.7, 22.5, 14.0 ppm; MS: *m*/*z* calcd for $C_{49}H_{51}N_2O_6$ $[M+H]^+$: 763.3747; found: 763.3749; elemental analysis calcd (%) for $C_{49}H_{50}N_2O_6$: C 77.14, H 6.61, N 3.67; found: C 77.41, H 6.89, N 3.41.

2.2.7. 4-Methoxy-N,N-bis[4-[N-(1-hexylheptyl)-6-anthraquinoneyl-2,3-dicarboxylic imide]-phenyl]benzenamine (*TPA-AQI2*)

Following general procedure B, compound **4** (0.64 g, 1.2 mmol), Na_2CO_3 (0.21 g, 2.0 mmol), $Pd(PPh_3)_4$ (60 mg) and compound **2b** (0.20 g, 0.55 mmol) were refluxed in a mixture of benzene (15 mL), ethanol (3 mL) and water (6 mL) under nitrogen. Silica gel column chromatography afforded the product **TPA-AQI2** (0.36 g, 55%) as red solids. ^{1}H NMR (400 MHz, $CDCl_3$): δ = 8.78 (s, 4H), 8.57 (d, J = 2.0 Hz, 2H), 8.41 (d, J = 8.0 Hz, 2H), 8.08 (q, J_1 = 8.0, J_2 = 2.0 Hz, 2H), 7.68 (d, J = 8.4 Hz, 4H), 7.26–7.18 (m, 6H), 6.96 (d, J = 9.2 Hz, 2H), 4.31–4.23 (m, 2H), 3.87 (s, 3H), 2.15–2.05 (m, 4H), 1.79–1.71 (m, 4H), 1.33–1.23 (m, 32H), 0.86 ppm (t, J = 6.4 Hz, 12H); ^{13}C NMR (100 MHz, $CDCl_3$): δ = 181.9, 181.1, 167.0, 146.9, 138.3, 138.1, 135.6, 135.5, 133.5, 132.2, 131.1, 128.6, 128.1, 125.2, 123.1, 123.0, 122.5, 122.4, 115.2, 115.1, 55.5, 53.2, 32.3, 31.7, 28.9, 26.7, 22.5, 14.0 ppm; MS: *m*/*z* calcd for $C_{77}H_{80}N_3O_9$ $[M+H]^+$: 1190.5895; found: 1190.5939; elemental analysis calcd (%) for $C_{77}H_{79}N_3O_9$: C 77.69, H 6.69, N 3.53; found: C 77.41, H 6.65, N 3.34.

2.2.8. Tri[4-[N-(1-hexylheptyl)-6-anthraquinoneyl-2,3-dicarboxylic imide]-phenyl]amine (*TPA-AQI3*)

Following general procedure B, compound **4** (0.85 g, 1.6 mmol), Na_2CO_3 (0.85 g, 8.0 mmol), $Pd(PPh_3)_4$ (100 mg) and compound **2c** (0.30 g, 0.48 mmol) were refluxed in a mixture of benzene (15 mL), ethanol (3 mL) and water (6 mL) under nitrogen. Silica gel column chromatography afforded the product **TPA-AQI3** (0.48 g, 62%) as black solids. ^{1}H NMR (400 MHz, $CDCl_3$): δ = 8.79 (d, J = 1.2 Hz, 6H), 8.60 (d, J = 1.2 Hz, 3H), 8.44 (d, J = 8.4 Hz, 3H), 8.12 (q, J_1 = 8.4 Hz, J_2 = 1.6 Hz, 3H), 7.76 (d, J = 8.4 Hz, 6H), 7.38 (d, J = 8.4 Hz, 6H), 4.32–4.24 (m, 3H), 2.15–2.06 (m, 6H), 1.78–1.72 (m, 6H), 1.29–1.24 (m, 48H), 0.86 ppm (t, J = 6.8 Hz, 18H); ^{13}C NMR (100 MHz, $CDCl_3$): δ = 181.8, 181.2, 167.0, 147.8, 146.7, 138.2, 138.0, 135.7, 135.5, 133.5, 132.4, 131.4, 128.7, 128.6, 125.4, 124.9, 124.8, 122.5, 111.5, 53.2, 32.3, 31.7, 28.9, 26.7, 22.5, 14.0 ppm; MS: *m*/*z* calcd for $C_{105}H_{109}N_4O_{12}$ $[M+H]^+$: 1617.8042; found: 1617.8084; elemental analysis calcd (%) for $C_{105}H_{108}N_4O_{12}$: C 77.94, H 6.73, N 3.46; found: C 78.08, H 6.54, N 3.29.

2.3. Electrochemical characterizations

Cyclic voltammetry was carried out on a CHI 840B electrochemical workstation. The solutions were made in CH_2Cl_2 containing 0.1 M tetra-n-butylammonium perchlorate (TBAP) as supporting electrolyte and were degassed with nitrogen prior to measurement. Glassy carbon was employed as the working electrode, platinum wire as the counter electrode and Ag/AgCl as the reference electrode. The pseudo-reference was calibrated externally using a 2–5 mM solution of ferrocene (Fc/Fc^+). The energy level of Fc/Fc^+ is assumed to be −4.8 eV below the vacuum level [64] and the LUMO levels of **TPA-AQI**, **TPA-AQI2** and **TPA-AQI3** were estimated from the half-wave potentials of the reduction peaks. Spectroelectrochemical measurements were carried out on a Hitachi U-4100 spectrophotometer connected to a computer in an optical transparent thin layer (OTTLE) cell. The solutions were as the same as for CV, and the redox potentials were chosen according to the results of CV.

2.4. Computational details

Molecular geometries were fully optimized using Kohn–Sham Density Functional Theory (DFT) based on the Becke's three parameter hybrid functional B3LYP [65] with the 6–31 G (d) basis set. Each optimization was verified by the frequency analysis. The frontier molecular orbital (MO) shapes and energy levels were calculated using the optimized structures. Time-dependent density functional theory (TD-DFT) was employed to stimulate the vertical transitions of the first 10 states using B3LYP/6-31G (d) basis set. All the calculations were performed using the Gaussian 09 program package [66] and the orbital pictures were prepared using Gaussview [67]. To simplify the calculations, methyl group was employed to replace the *N*-1-hexylheptyl groups.

3. Results and discussion

3.1. Synthesis

The synthetic route of the three star-shaped D-A molecules is illustrated in Scheme 1. The bromine substituted triphenylamine **1** were transferred to corresponding boronic ester **2** firstly with *n*-BuLi and then 2-isopropoxy-4,4,5,5-tetramethyl-[1,3,2]dioxaborolane. Classic palladium-catalyzed Suzuki-coupling reactions between corresponding boronic ester **2** and 6-bromo substituted anthraquinone imide **4** afforded the three target star-shaped molecules (namely, **TPA-AQI**, **TPA-AQI2** and **TPA-AQI3**). The long hexylheptyl group as well as the propeller-like structures of the molecules ensure the solubility of these molecules in common organic solvents such as dichloromethane, chloroform and toluene. 4-Methoxyl group was incorporated at the *para*-position of phenyl groups of TPA unit in **TPA-AQI** and **TPA-AQI2** to reduce the oxidation potential and also stabilize the corresponding radical cations as mentioned above.

The chemical structures of these molecules were fully confirmed by ^{1}H NMR, high resolution mass spectrometry and elemental analysis. As revealed in the ^{1}H NMR spectra (Fig. S1), chemical shifts of the aromatic protons in TPA segment were moved gradually toward the low field with increasing **AQI** arms connected to it owing to the electron-withdrawing nature of **AQI** group, while the chemical shifts of the aromatic protons in **AQI** segment were much less influenced.

3.2. Photophysical properties

Absorption spectra of compounds **TPA-AQI**, **TPA-AQI2** and **TPA-AQI3** in dilute CH_2Cl_2 solutions are shown in Fig. 1. There are two groups of absorption bands between 300 and 700 nm for the molecules solution. The intense and weakly structured absorption bands in the range of 300–450 nm correspond to the π–π^* transitions. And, the visible absorption bands can be assigned to an intramolecular charge transfer (ICT) from the donor (TPA) to the acceptor (AQI) [68].

Comparison of the spectra of **TPA-AQI**, **TPA-AQI2** and **TPA-AQI3** shows that the progressive incorporation of AQI arm onto TPA core induces a concomitant increase of the intensity of the π–π^* transition and ICT band. Another noteworthy is the hypsochromic shift of ICT bands. As for **TPA-AQI3**, the ICT based absorption band occurs at about 504 nm, while that of **TPA-AQI** and **TPA-AQI2** at 542 nm and 522 nm, respectively. This phenomenon could be ascribed to the strong molecular polarity of **TPA-AQI** and **TPA-AQI2** which favors the ICT electron delocalization [69], and also the increased steric hindrance in **TPA-AQI3** as indicated in the optimized geometries obtained by density-functional theory (DFT) at the B3LYP/6-31 G (d) level (Fig. 2). With the increasing number of AQI arms, dihedral

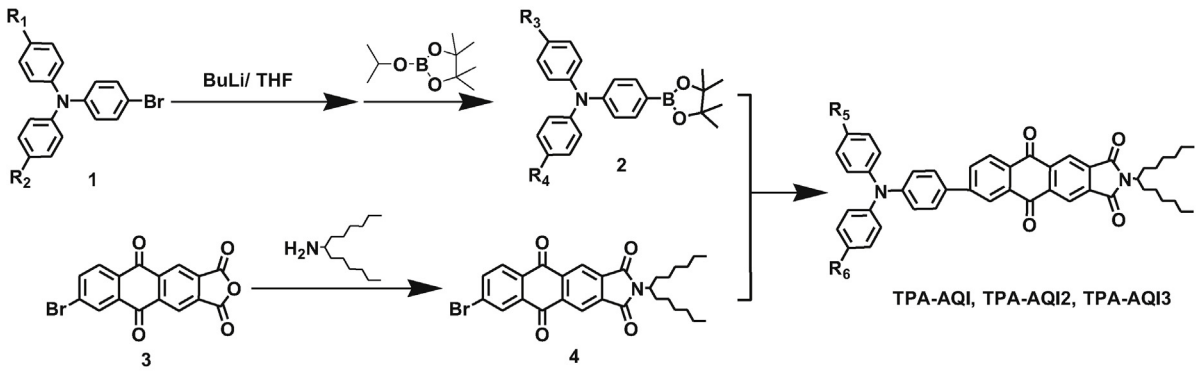

	R_1	R_2		R_3	R_4		R_5	R_6
1a	OCH_3	OCH_3	**2a**	OCH_3	OCH_3	**TPA-AQI**	OCH_3	OCH_3
1b	OCH_3	Br	**2b**	OCH_3	M1	**TPA-AQI2**	OCH_3	M2
1c	Br	Br	**2c**	M1	M1	**TPA-AQI3**	M2	M2

Scheme 1. Synthetic route of star-shaped molecules **TPA-AQI**, **TPA-AQI2** and **TPA-AQI3**.

angles between the donor and acceptor segments are enlarged, which reduces the conjugation degree and thereby increases the HOMO (highest occupied molecular orbital)-LUMO (lowest unoccupied molecular orbital) gap as revealed in Fig. 2.

The intrinsic characters of these absorptions are also revealed by the TD-DFT calculations. The calculated absorptions and corresponding transitions are illustrated in Fig. S2 and Table S1, respectively. It is calculated that the lowest-energy absorptions have a nature of charge transfer. For the single branched molecule **TPA-AQI**, the $S_0 \rightarrow S_1$ excitation is pure HOMO → LUMO transition, with the HOMO and LUMO orbitals concentrated on the donor and acceptor moieties, respectively (Fig. 2). With an increase of AQI arms as in **TPA-AQI2** and **TPA-AQI3**, a second CT excitation ($S_0 \rightarrow S_2$) is present in the CT band. This $S_0 \rightarrow S_2$ excitation is due to the HOMO → LUMO + 1 transition. As shown in Fig. 2, it is meaningful to point out that the LUMO and LUMO + 1 orbitals of **TPA-AQI2** are the in-phase and out-of-phase combinations of the local LUMO orbital of each AQI arm [70]. The superposition of these two CT transitions well explains the linearly increasing intensity of the charge-transfer bands from **TPA-AQI** to **TPA-AQI3**.

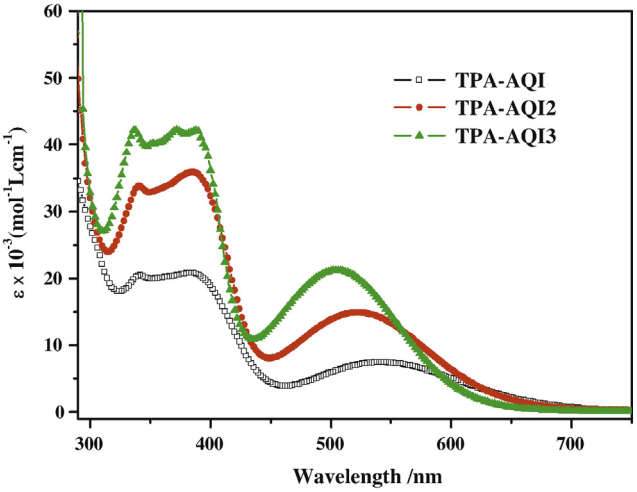

Fig. 1. UV–vis spectra of the three compounds in dilute CH_2Cl_2.

3.3. Electrochemical properties

Cyclic voltammetry (CV) is a preliminary measurement to determine the redox properties of organic and polymeric materials. The redox properties of these three molecules were investigated by CV measurement in CH_2Cl_2 solutions with tetra-*n*-butylammonium perchlorate (TBAP) as supporting electrolyte. As shown in Fig. 3, the CV curves of all compounds are similar and there are three reduction/oxidation processes. In the cathodic regime, there are two quasi-reversible characteristic reduction peaks of AQI moiety, corresponding to the formation of radical anions and dianions, respectively. And in the anodic side, the oxidation process is related to the oxidation of the TPA group to form radical cations.

As also exhibited in the CV curves, these compounds show almost the same reduction potentials, indicating the negligible influence of TPA group on AQI moiety, which is consistent with the chemical shifts of the aromatic protons in **TPA** segment. However, the cathodic current increases linearly with AQI arms, which is understandable considering the simultaneous electrochemical process in different branches. In contrast, the oxidation peaks in the positive regime are dramatically influenced and shift toward more positive region with the increase of AQI arms, indicating the progressive stabilization of the HOMO level due to the electron-withdrawing characteristic of AQI group.

The redox potentials (vs Ag/AgCl) of these compounds as well as the unsubstituted **AQI** are summarized in Table 1. As demonstrated in Table 1, all these compounds share almost the same reduction potential, while the oxidation potentials shift to more and more positive. The frontier MO energies and band-gaps calculated from the electrochemical results are also listed in Table 1. The HOMO level of **TPA-AQI3** is largely stabilized as compared to **TPA-AQI**. The band-gap of each these molecules is in the range of 1.43–1.75 eV, which agrees with the broad absorption of these compounds and is beneficial for photovoltaic applications [71]. These experimental results show considerable consistency with the theoretical ones as illustrated in Fig. 2. And the differences between experimental and theoretical values are a well-known consequence of the lack of medium-related factors in calculations.

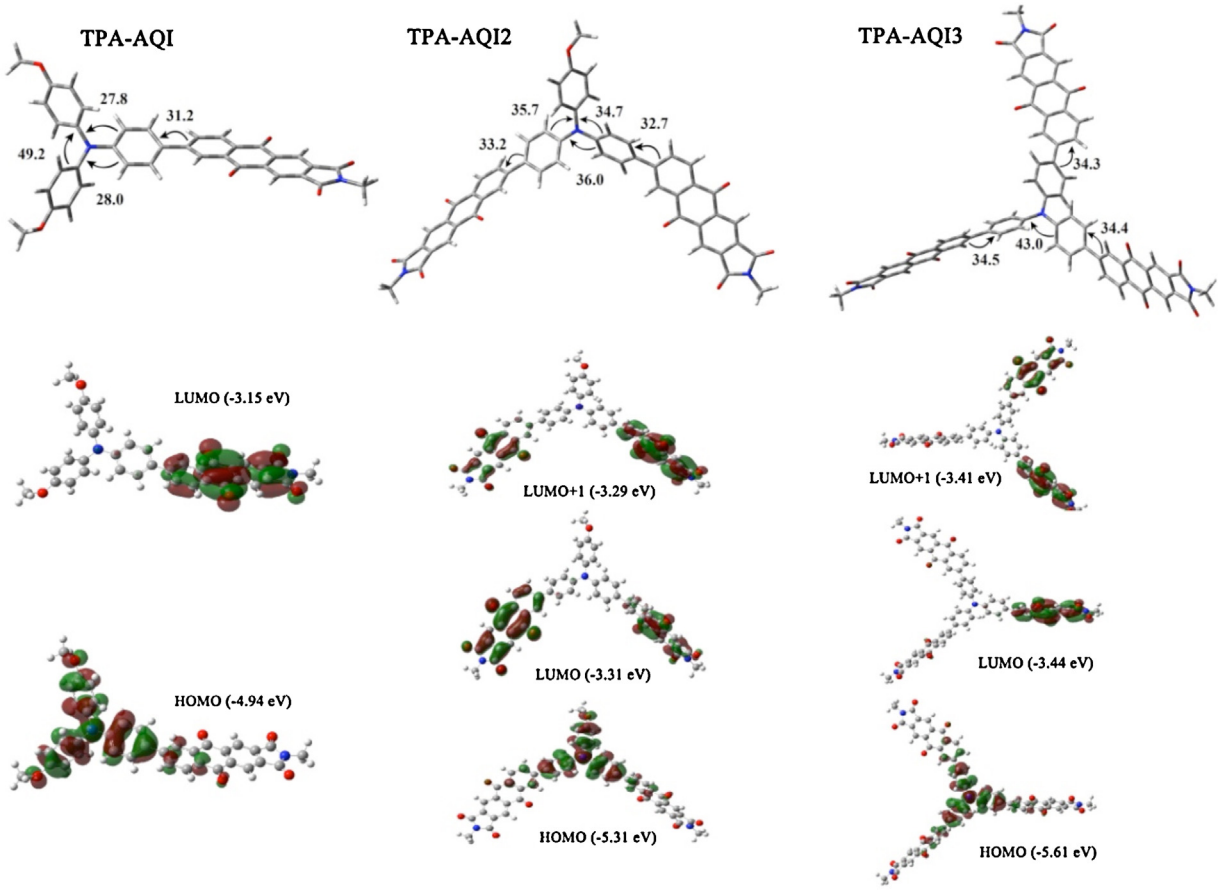

Fig. 2. Optimized geometries and frontier MOs with corresponding energy levels of the compounds obtained at the B3LYP/6-31 G (d) level.

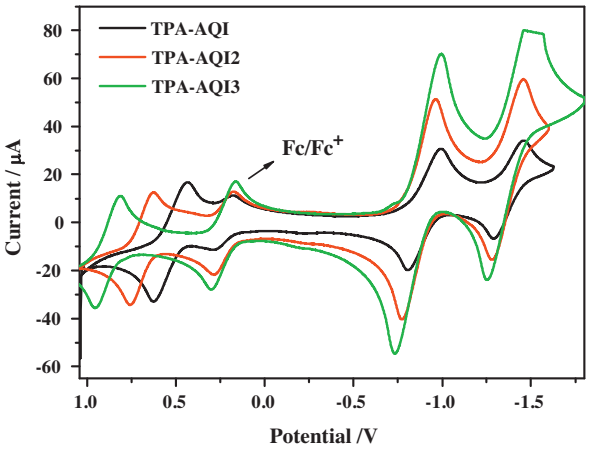

Fig. 3. Cyclic voltammograms of the compounds (1.0 mM) recorded in a CH_2Cl_2 solution of Bu_4NClO_4 (0.10 M) at a scanning rate of 100 mV/s (vs Ag/AgCl).

3.4. Spectroelectrochemical characterization

Spectroelectrochemical measurements are carried out using the OTTLE cell to investigate the electrochromic properties and the typical electrochromic behaviors of **TPA-AQI** are demonstrated in Fig. 4. In the neutral state, besides the absorption in the UV region, there is another structureless ICT based absorption centered at 542 nm. When applied a positive potential of 0.8 V, this ICT absorption disappeared gradually and three new peaks in the visible region centered at 500 nm, 626 nm and 764 nm, corresponding to the formation of TPA radical cations [72], appeared. Meanwhile, the solution color changes from Indian-red to bluish green due the disruption of the ICT absorption (Fig. 4a). When a low negative potential was applied, the radical cations were reduced to the neutral state and the ICT absorption re-appeared with the solution color returning to Indian-red (Fig. 4b). A similar effect is observed during reduction of **TPA-AQI** to its radical anions when the applied negative potential was increased: the ICT absorption disappeared again and a broad NIR absorption ranging from 700 to 1100 nm turned up together with the color changing to olive green (Fig. 4c).

Table 1
Redox potentials[a] and related MO energies of the compounds.

Comp.	E_{ox}/V	$E_{red}{}^1$/V	$E_{red}{}^2$/V	E_{HOMO}/eV [b]	E_{LUMO}/eV [b]	E_g/eV [c]
TPA-AQI	0.53	−0.90	−1.38	−5.10	−3.67	1.43
TPA-AQI2	0.69	−0.87	−1.37	−5.26	−3.70	1.56
TPA-AQI3	0.89	−0.86	−1.36	−5.46	−3.71	1.75
AQI [d]	–	−0.86	−1.34	–	−3.71	–

[a] $c = 1 \times 10^{-3}$ mol/L in CH_2Cl_2/TBAP (0.1 M) vs Ag/AgCl at 100 mV/s.
[b] LUMO (eV) = $-(E_{red}{}^1 - E_{Fc/Fc^+} + 4.8)$ (eV), HOMO (eV) = $-(E_{ox} - E_{Fc/Fc^+} + 4.8)$ (eV).
[c] E_g = LUMO-HOMO.
[d] CV results for unsubstituted **AQI**.

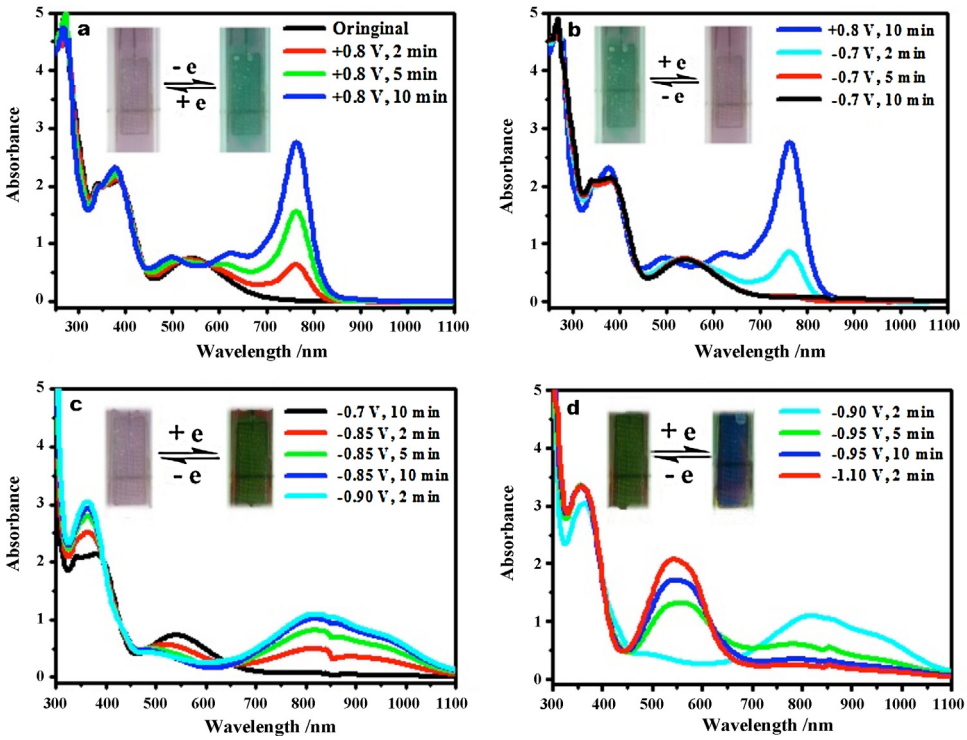

Fig. 4. UV–vis–NIR spectra of **TPA-AQI** (1.0 mM containing 0.1 M Bu_4NClO_4) at different redox states in CH_2Cl_2 (inset: photos at different states).

The assignment of this NIR absorption was indicated by the TD-DFT calculation results (Table 2).

As shown in Table 2, the first two lowest-energy transitions both have a combined contribution from the SOMO → LUMO transition and SOMO → LUMO + 2 transition. Due to the smaller calculated oscillator strength, the calculated first lowest energy absorption at 953 nm was observed as a side-band in the experimental spectra as indicated Fig. 4c. The observed NIR absorption of **TPA-AQI** radical cations was simulated to result from transitions from the internal orbitals to LUMO (HOMO-1 → LUMO and HOMO-3 → LUMO, Table 2). And the calculated NIR absorptions are presented in Fig. S3. The NIR absorption of the AQI radical anions could be transferred to the absorption of dianions by application of even higher negative potentials, which showed intensive absorption from 450 to 700 nm, corresponding to the generated dark-blue color (Fig. 4d).

These results show that the ICT interactions can be modulated by both the oxidation of the TPA core as well as the reduction of the AQI arms, and multicolor switching also can be achieved electrochemically. The other two molecules demonstrate the similar electrochromic behaviors (Fig. S4). Due to the ambipolar characteristics of these compounds, an all-solid state EC device based on molecule **TPA-AQI** was fabricated as a typical example (Fig. S5). When a positive potential was applied to the device, a new absorption around 800 nm appeared while a broad NIR absorption appeared when the potential changed to a negative one, which is the same as that in the solution. The optical switching properties at 800 nm and 900 nm were also measured and an optical contrast of 23% was achieved at 800 nm (Fig. S6).

Table 2
Calculated excitation energy (ΔE), oscillator strength (f) and dominant transitions of the first 10 main predicted transitions of **TPA-AQI** radical cations and anions (H: HOMO; L: LUMO; S: SOMO, single occupied molecular orbital).*

S_n	ΔE(eV, nm)	f	Dominant transitions (%)
Radical cations			
S_2	1.56, 795	0.136	H-1->L β (82%), H-3->L β (15%)
S_3	1.66, 746	0.112	H-2->L β (57%), H-3->L β (28%)
S_4	1.68, 738	0.081	H-3->L β (52%), H-2->L β (38%)
S_5	1.79, 693	0.231	H-6->L β (97%)
Radical anions			
S_1	1.30, 953	0.127	S->L α (73%), S->L + 2 α (18%)
S_2	1.50, 824	0.186	S->L + 2 α (63%), H->L α (25%)

* Only those transitions with $f > 0.01$ are listed.

4. Conclusion

In summary, three D-A molecules with different AQI arms connected to TPA core were synthesized and characterized. Their optical, electrochemical, spectroelectrochemical properties were studied and discussed in terms of correlation with their chemical structures. Due to the propeller-like structures, these compounds show good solubility in common organic solvents. In the absorption spectra of dilute CH_2Cl_2 solutions, there are two main absorption bands with the lower energy absorption corresponding to the intramolecular charge transfer from the electron-donating TPA unit to the electron-accepting AQI unit and the higher energy absorption assigned to the π–π^* transition. With increasing the AQI arms, an enhancement of the absorption intensity and hypsochromic shift of ICT band were observed, which may result from the increased steric hindrance. The experimental optical properties agree well with the theoretical calculated neutral absorptions. All these molecules show broad absorptions and narrow band-gaps, which may find applications in optoelectronic fields. CV results reveal that all these compounds exhibit three redox peaks, two in the cathodic regime which corresponds to the formation of AQI radical anions and dianions, respectively, one in the positive regime corresponding to the TPA radical cations. Spectroelectrochemical measurements demonstrate that the ICT based absorption could be tuned electrochemically and multi-color electrochromism can be achieved in one single molecule. When oxidized to radical cations or reduced to radical anions, intensive NIR absorptions were measured. According to the simulation results, the origin of NIR absorption for **TPA-AQI** radical cations has a nature of transitions from internal orbitals (HOMO-1 and HOMO-3) to LUMO, while from SOMO to LUMO and LUMO + 2 for radical anions.

Acknowledgement

We thank the financial support of the National Natural Science Foundation of China (No. 20834001) and the Research Fund for Doctoral Program of Higher Education of MOE of China (No. 20060001029).

Appendix A. Supplementary data

Supplementary data associated with this article can be found, in the online version, at http://dx.doi.org/10.1016/j.electacta.2013.03.067.

References

[1] R.J. Mortimer, Electrochromic materials, Chemical Society Reviews 26 (1997) 147.
[2] P.M.S. Monk, R.J. Mortimer, D.R. Rosseinsky, Electrochromism: Fundamentals and Applications, VCH, Weinheim, 1995.
[3] Y.G. Ko, W. Kwon, H.J. Yen, C.W. Chang, D.M. Kim, K. Kim, S.G. Hahm, T.J. Lee, G.S. Liou, M. Ree, Various digital memory behaviors of functional aromatic polyimides based on electron donor and acceptor substituted triphenylamines, Macromolecules 45 (2012) 3749.
[4] T.L. Choi, K.H. Lee, W.J. Joo, S. Lee, T.W. Lee, M.Y. Chae, Synthesis and nonvolatile memory behavior of redox-active conjugated polymer-containing ferrocene, Journal of the American Chemical Society 129 (2007) 9842.
[5] S. Moller, C. Perlov, W. Jackson, C. Taussig, S.R. Forrest, A polymer/semiconductor write-once read-many-times memory, Nature 426 (2003) 166.
[6] R. Baetens, B.P. Jelle, A. Gustavsen, Properties, requirements and possibilities of smart windows for dynamic daylight and solar energy control in buildings: a state-of-the-art review, Solar Energy Materials and Solar Cells 94 (2010) 87.
[7] G.A. Niklasson, C.G. Granqvist, Electrochromics for smart windows: thin films of tungsten oxide and nickel oxide, and devices based on these, Journal of Materials Chemistry 17 (2007) 127.
[8] R.D. Rauh, Electrochromic windows: an overview, Electrochimica Acta 44 (1999) 3165.
[9] R.J. Mortimer, A.L. Dyer, J.R. Reynolds, Electrochromic organic and polymeric materials for display applications, Dentessence 27 (2006) 2.
[10] P.M.S. Monk, The effect of ferrocyanide on the performance of heptyl viologen-based electrochromic display devices, Journal of Electroanalytical Chemistry 432 (1997) 175.
[11] C.G. Granqvist, Handbook of Inorganic Electrochromic Materials, Elsevier, Amsterdam, 1995.
[12] G. Wang, X.K. Fu, J. Huang, C.L. Wu, L. Wu, Q.L. Du, Synthesis of a new star-shaped 4,4′-bipyridine derivative and its multicolor solid electrochromic devices, Organic Electronics 12 (2011) 1216.
[13] J. Luo, Y.G. Ma, J. Pei, Y.L. Song, Recent progress on organic and polymeric electrochromic materials, Current Physical Chemistry 1 (2011) 216.
[14] A.L. Dyer, J.R. Reynolds, Electrochromism of conjugated conducting polymers, in: T.A. Skotheim, J.R. Reynolds (Eds.), Handbook of Conducting Polymers, vol. 1, CRC Press, Boca Raton, FL, 2007, p. 1, Ch. 20.
[15] G. Sonmez, H. Meng, F. Wudl, Organic polymeric electrochromic devices: polychromism with very high coloration efficiency, Chemistry of Materials 16 (2004) 574.
[16] E. Kaya, A. Balan, D. Baran, A. Cirpan, L. Toppare, Electrochromic and optical studies of solution processable benzotriazole and fluorene containing copolymers, Organic Electronics 12 (2011) 202.
[17] H.C. Ko, S. Kim, H. Lee, B. Moon, Multicolored electrochromism of a poly{1,4-bis[2-(3,4-ethylenedioxy)thienyl]benzene} derivative bearing viologen functional groups, Advanced Functional Materials 15 (2005) 905.
[18] A.A. Argun, P.H. Aubert, B.C. Thompson, I. Schwendeman, C.L. Gaupp, J. Hwang, N.J. Pinto, D.B. Tanner, A.G. MacDiarmid, J.R. Reynolds, Multicolored electrochromism in polymers: structures and devices, Chemistry of Materials 16 (2004) 4401.
[19] G. Sonmez, Polymeric electrochromics, Chemical Communications (2005) 5251.
[20] H.M. Wang, S.H. Hsiao, Multicolor electrochromic poly(amide-imide)s with N,N-diphenyl-N′,N′-di-4-tert-butylphenyl-1,4-phenylenediamine moieties, Polymer Chemistry 1 (2010) 1013.
[21] A. Cihaner, F. Algı, A novel neutral state green polymeric electrochromic with superior n- and p-doping processes: closer to red-blue-green (RGB) display realization, Advanced Functional Materials 18 (2008) 3583.
[22] P.M. Beaujuge, S. Ellinger, J.R. Reynolds, The donor–acceptor approach allows a black-to-transmissive switching polymeric electrochrome, Nature Materials 7 (2008) 795.
[23] P.M. Beaujuge, J.R. Reynolds, Color control in π-conjugated organic polymers for use in electrochromic devices, Chemical Reviews 110 (2010) 268.
[24] C.M. Amb, A.L. Dyer, J.R. Reynolds, Navigating the color palette of solution processable electrochromic polymers, Chemistry of Materials 23 (2011) 397.
[25] A.L. Dyer, E.J. Thompson, J.R. Reynolds, Completing the color palette with spray-processable polymer electrochromics, ACS Applied Materials & Interfaces 3 (2011) 1787.
[26] G. Qian, Z.Y. Wang, Near-infrared organic compounds and emerging applications, Chemistry – An Asian Journal 5 (2010) 1006.
[27] G. LeClair, Z.Y. Wang, Optical attenuation at the 1550-nm wavelength in a reflective mode using electrochromic ruthenium complex film, Journal of Solid State Electrochemistry 13 (2009) 365.
[28] M. Ward, Near-infrared electrochromic materials for optical attenuation based on transition-metal coordination complexes, Journal of Solid State Electrochemistry 9 (2005) 778.
[29] J. Fabian, H. Nakazumi, M. Matsuoka, Near-infrared absorbing dyes, Chemical Reviews 92 (1992) 1197.
[30] C.J. Yao, Y.W. Zhong, H.J. Nie, H.D. Abruna, J.N. Yao, Near-IR, electrochromism in electropolymerized films of a biscyclometalated ruthenium complex bridged by 1,2,4,5-tetra(2-pyridyl)benzene, Journal of the American Chemical Society 133 (2011) 20720.
[31] W. Kaim, Concepts for metal complex chromophors absorbing in the near infrared, Coordination Chemistry Reviews 255 (2011) 2503.
[32] S. Wang, X.Z. Li, S.D. Xun, X.H. Wan, Z.Y. Wang, Near-infrared electrochromic and electroluminescent polymers containing pendant ruthenium complex groups, Macromolecules 39 (2006) 7502.
[33] S. Wang, E.K. Todd, M. Birau, J. Zhang, X.H. Wan, Z.Y. Wang, Near-infrared electrochromism in electroactive pentacenediquinone-containing poly(caryl ether)s, Chemistry of Materials 17 (2005) 6388.
[34] J.E. Almlof, M.W. Feyereisen, T.H. Jozefiak, L.L. Miller, Electronic structure and near-infrared spectra of diquinone anion radicals, Journal of the American Chemical Society 112 (1990) 1206.
[35] E.N. Esmer, S. Tarkuc, Y.A. Udum, L. Toppare, Near infrared electrochromic polymers based on phenazine moieties, Materials Chemistry and Physics 131 (2011) 519.
[36] H.J. Yen, G.S. Liou, Enhanced near-infrared electrochromism in triphenylamine-based aramids bearing phenothiazine redox centers, Journal of Materials Chemistry 20 (2010) 9886.
[37] A.L. Dyer, C.R.G. Grenier, J.R. Reynolds, A poly(3,4-alkylenedioxythiophene) electrochromic variable optical attenuator with near-infrared reflectivity tuned independently of the visible region, Advanced Functional Materials 17 (2007) 1480.
[38] H. Meng, D. Tucker, S. Chaffins, Y. Chen, R. Helgeson, B. Dunn, F. Wudl, An unusual electrochromic device based on a new low-bandgap conjugated polymer, Advanced Materials 15 (2003) 146.
[39] J. Zheng, W.Q. Qiao, X.H. Wan, J.P. Gao, Z.Y. Wang, Near-infrared electrochromic and chiroptical switching materials: design, synthesis, and characterization of chiral organogels containing stacked naphthalene diimide chromophores, Chemistry of Materials 20 (2008) 6163.
[40] J.F. Penneau, L.L. Miller, An imide radical anion which assembles into π-stacks in solution, Angewandte Chemie International Edition 30 (1991) 986.
[41] S.F. Rak, T.H. Jozefiak, L.L. Miller, Electrochemistry and near-infrared spectra of anion radicals containing several imide or quinone groups, Journal of Organic Chemistry 55 (1990) 4794.
[42] Y.J. Zheng, J.X. Cui, J. Zheng, X.H. Wan, Near-infrared electrochromic and chiroptical switching polymers: synthesis and characterization of helical poly(N-propargylamides) carrying anthraquinone imide moieties in side chains, Journal of Materials Chemistry 20 (2010) 5915.
[43] Y.J. Zheng, J. Zheng, L.T. Dou, W.Q. Qiao, X.H. Wan, Synthesis and characterization of a novel kind of near-infrared electrochromic polymers containing anthraquinone imide group and ionic moieties, Journal of Materials Chemistry 19 (2009) 8470.
[44] W.Q. Qiao, J. Zheng, Y.F. Wang, Y.J. Zheng, N.H. Song, X.H. Wan, Z.Y. Wang, Efficient synthesis and properties of novel near-infrared electrochromic anthraquinone imides, Organic Letters 10 (2008) 641.
[45] F.K. Chen, J. Zhang, H. Jiang, X.H. Wan, Novel colorless to purplish-red switching electrochromic anthraquinone imide with broad vis-NIR absorptions in radical anion state: simulation aided molecular design, Chemistry-An Asian Journal (2013), http://dx.doi.org/10.1002/asia.201300176.
[46] Y. Shirota, H. Kageyama, Charge carrier transporting molecular materials and their applications in devices, Chemical Reviews 107 (2007) 953.
[47] S. Roquet, A. Cravino, P. Leriche, O. Alévêque, P. Frère, J. Roncali, Triphenylamine–thienylenevinylene hybrid systems with internal charge transfer as donor materials for heterojunction solar cells, Journal of the American Chemical Society 128 (2006) 3459.
[48] Y. Shirota, Photo- and electroactive amorphous molecular materials – molecular design, syntheses, reactions, properties, and applications, Journal of Materials Chemistry 15 (2005) 75.
[49] D. Deng, Y. Yang, J. Zhang, C. He, M.J. Zhang, Z.G. Zhang, Z.J. Zhang, Y.F. Li, Triphenylamine-containing linear D-A-D molecules with benzothiadiazole as acceptor unit for bulk-heterojunction organic solar cells, Organic Electronics 12 (2011) 614.
[50] E.T. Seo, R.F. Nelson, J.M. Fritsch, L.S. Marcoux, D.W. Leedy, R.N. Adams, Anodic oxidation pathways of aromatic amines. Electrochemical and electron paramagnetic resonance studies, Journal of the American Chemical Society 88 (1966) 3498.
[51] S. Beaupré, J. Dumas, M. Leclerc, Toward the development of new textile/plastic electrochromic cells using triphenylamine-based copolymers, Chemistry of Materials 18 (2006) 4011.

[52] M.K. Leung, M.Y. Chou, Y.O. Su, C.L. Chiang, H.L. Chen, C.F. Yang, C.C. Yang, C.C. Lin, H.T. Chen, Diphenylamino group as an effective handle to conjugated donor-acceptor polymers through electropolymerization, Organic Letters 5 (2003) 839.
[53] M. Ouyang, G.C. Wang, C. Zhang, A novel electrochromic polymer containing triphenylamine derivative and pyrrole, Electrochimica Acta 56 (2011) 4645.
[54] S.H. Cheng, S.H. Hsiao, T.H. Su, G.S. Liou, Novel aromatic poly(amine-imide)s bearing a pendent triphenylamine group: synthesis, thermal, photophysical, electrochemical, and electrochromic characteristics, Macromolecules 38 (2005) 307.
[55] H.J. Yen, H.Y. Lin, G.S. Liou, Novel starburst triarylamine-containing electroactive aramids with highly stable electrochromism in near-infrared and visible light regions, Chemistry of Materials 23 (2011) 1874.
[56] H.J. Yen, G.S. Liou, Solution-processable triarylamine-based electroactive high performance polymers for anodically electrochromic applications, Polymer Chemistry 3 (2012) 255.
[57] L.T. Huang, H.J. Yen, J.H. Wu, G.S. Liou, Preparation and characterization of near-infrared and multi-colored electrochromic aramids based on aniline-derivatives, Organic Electronics 13 (2012) 840.
[58] G.S. Liou, C.W. Chang, Highly stable anodic electrochromic aromatic polyamides containing N,N,N',N'-tetraphenyl-p-phenylenediamine moieties: synthesis, electrochemical, and electrochromic properties, Macromolecules 41 (2008) 1667.
[59] C.W. Chang, G.S. Liou, S.H. Hsiao, Highly stable anodic green electrochromic aromatic polyamides: synthesis and electrochromic properties, Journal of Materials Chemistry 17 (2007) 1007.
[60] Y.J. Chang, T.J. Chow, Triaryl linked donor acceptor dyads for high-performance dye-sensitized solar cells, Tetrahedron 65 (2009) 9626.
[61] C. Teng, X. Yang, C. Yang, S. Li, M. Cheng, A. Hagfeldt, L. Sun, Molecular design of anthracene-bridged metal-free organic dyes for efficient dye-sensitized solar cells, Journal of Physical Chemistry C 114 (2010) 9101.
[62] J. Cremer, P. Bauerle, Star-shaped perylene–oligothiophene–triphenylamine hybrid systems for photovoltaic applications, Journal of Materials Chemistry 16 (2006) 874.
[63] F.K. Chen, J. Zhang, X.H. Wan, Design and synthesis of piezochromic materials based on push–pull chromophores: a mechanistic perspective, Chemistry-A European Journal 18 (2012) 4558.
[64] J. Pommerehne, H. Vestweber, W. Guss, R.F. Mahrt, H. Bässler, M. Porsch, J. Daub, Efficient two layer leds on a polymer blend basis, Advanced Materials 7 (1995) 551.
[65] A.D. Becke, Density-functional thermochemistry. III. The role of exact exchange, Journal of Chemical Physics 98 (1993) 5648.
[66] M.J. Frisch, G.W. Trucks, H.B. Schlegel, G.E. Scuseria, M.A. Robb, J.R. Cheeseman, G. Scalmani, V. Barone, B. Mennucci, G.A. Petersson, H. Nakatsuji, M. Caricato, X. Li, H.P. Hratchian, A.F. Izmaylov, J. Bloino, G. Zheng, J.L. Sonnenberg, M. Hada, M. Ehara, K. Toyota, R. Fukuda, J. Hasegawa, M. Ishida, T. Nakajima, Y. Honda, O. Kitao, H. Nakai, T. Vreven, J.A. Montgomery Jr., J.E. Peralta, F. Ogliaro, M. Bearpark, J.J. Heyd, E. Brothers, K.N. Kudin, V.N. Staroverov, R. Kobayashi, J. Normand, K. Raghavachari, A. Rendell, J.C. Burant, S.S. Iyengar, J. Tomasi, M. Cossi, N. Rega, J.M. Millam, M. Klene, J.E. Knox, J.B. Cross, V. Bakken, C. Adamo, J. Jaramillo, R. Gomperts, R.E. Stratmann, O. Yazyev, A.J. Austin, R. Cammi, C. Pomelli, J.W. Ochterski, R.L. Martin, K. Morokuma, V.G. Zakrzewski, G.A. Voth, P. Salvador, J.J. Dannenberg, S. Dapprich, A.D. Daniels, O. Farkas, J.B. Foresman, J.V. Ortiz, J. Cioslowski, D.J. Fox, Gaussian 09, in: Revision A. 02, Gaussian, Inc, Wallingford CT, 2009.
[67] R. Dennington, T. Keith, J. Millam, Gauss View, Version 5.0.8, Semichem Inc, Shawnee Mission KS, 2009.
[68] Y. Yang, J. Zhang, Y. Zhou, G. Zhao, C. He, Y. Li, M. Andersson, O. Inganäs, F. Zhang, Solution-processable organic molecule with triphenylamine core and two benzothiadiazole-thiophene arms for photovoltaic application, Journal of Physical Chemistry C 114 (2010) 3701.
[69] T. Duan, K. Fan, Y. Fu, C. Zhong, X. Chen, T. Peng, J. Qin, Triphenylamine-based organic dyes containing a 1,2,3-triazole bridge for dye-sensitized solar cells via a 'Click' reaction, Dyes Pigments 94 (2012) 28.
[70] D. Gudeika, A. Michaleviciute, J.V. Grazulevicius, R. Lygaitis, S. Grigalevicius, V. Jankauskas, A. Miasojedovas, S. Jursenas, G. Sini, Structure properties relationship of Donor–Acceptor derivatives of triphenylamine and 1,8-naphthalimide, Journal of Physical Chemistry C 116 (2012) 14811.
[71] M.C. Scharber, D. Mühlbacher, M. Koppe, P. Denk, C. Waldauf, A.J. Heeger, C.J. Brabec, Design rules for donors in bulk-heterojunction solar cells – towards 10% energy-conversion efficiency, Advanced Materials 18 (2006) 789.
[72] F.A. Neugebauer, S. Bamberger, W.R. Groh, Mono-, di-, and triarylamine radical cations, Chemische Berichte 108 (1975) 2406.